April 2004

Mathematical modeling and field evaluation of embankment stabilized with vertical drains incorporating vacuum preloading

Buddhima Indraratna
University of Wollongong, indra@uow.edu.au

Cholachat Rujikiatkamjorn
University of Wollongong, cholacha@uow.edu.au


Proceedings: Fifth International Conference on Case Histories in Geotechnical Engineering
New York, NY, April 13-17, 2004

MATHEMATICAL MODELING AND FIELD EVALUATION OF EMBANKMENT STABILIZED WITH VERTICAL DRAINS INCORPORATING VACUUM PRELOADING

Buddhima Indraratna
Professor of Civil Engineering,
University of Wollongong
Wollongong, NSW 2522, Australia

Cholachat Rujikiatkamjorn
Division of Civil Engineering,
University of Wollongong
Wollongong, NSW 2522, Australia

ABSTRACT

This study presents the analytical modeling of vertical drains incorporating vacuum preloading in both axisymmetric and plane strain conditions. The effectiveness of vacuum pressure (i.e. both constant vacuum pressure and varied vacuum pressure) applied along the drain is considered. A multidrain plane strain model is employed to analyse an embankment at the site of Second Bangkok International Airport (SBIA) stabilised with prefabricated vertical drains. At this site, a significantly reduced height of sand surcharge was applied by reducing the pore pressures through vacuum preloading. The results of FEM analysis confirm the efficiency of vacuum preloading in comparison with the conventional method of surcharge alone.

INTRODUCTION

In recent years, prefabricated band drains have been used widely for soft ground improvement. Radial drainage accelerates soft soil consolidation. Baron (1948) and Hansbo (1981) introduced the unit cell theory for axisymmetric and plane strain conditions. Subsequently, the unit cell theory was extended by including a smear zone, which occurs when surrounding soil is remoulded during the vertical drain installation (Hird et al., 1992). Due to the increasing popularity of plane strain finite element analysis, Indraratna and Redana (1997) extended the equivalent unit cell theory to convert the axisymmetric parameters such as permeability into equivalent plane strain parameters. As a result, the plane strain finite element analyses have been used extensively to predict the behaviour of embankments improved by prefabricated vertical drains (e.g. Indraratna and Redana, 2000).

In order to increase the rate of consolidation, Kjellman (1952) introduced the concept of vacuum preloading to improve the soil strength. Recently, the system of vertical drains enhanced by incorporating vacuum preloading has been applied in land reclamation projects (Shang et al., 1998, Chu, et al., 2000). Mohamedelhassan and Shang (2002) discussed the application of vacuum pressure and its benefits, but without any prefabricated vertical drains (PVD). The benefits of this method include accelerating consolidation by increasing the hydraulic gradient and reducing the height of the embankment to achieve the same degree of consolidation.

In this study, analytical solutions for a single drain incorporating vacuum preloading in both axisymmetric and plane strain conditions are introduced. In order to compare the efficiency of vacuum preloading, various possible distribution patterns of vacuum pressure via the vertical drain system are discussed. Finally, the equivalent plane strain model in conjunction with the modified Cam-Clay theory is applied to 2 embankments at the Second Bangkok International Airport (SBIA).

ANALYTICAL SOLUTIONS FOR VERTICAL DRAIN INCORPORATING VACUUM PRELOADING AND SMEAR EFFECTS

In this section, the analytical solutions of unit cell for axisymmetric and plane strain conditions are revised from the original theory developed by Hird et al. (1992) and Indraratna and Redana (1997). Figures 1a and 1b illustrate the unit cell adopted for the axisymmetric and plane strain conditions, respectively. The efficiency of vacuum preloading is taken into account by dividing the distribution pattern of vacuum pressure into 4 distinct categories (Fig. 2):

Case A: Vacuum pressure is constant along the drain and across the soil element.

Case B: Vacuum pressure is constant along the drain while it varies linearly to zero across the soil element. This represents a large drain spacing but relatively short drain lengths.

Case C: Vacuum pressure varies linearly along the drain while remaining constant across the soil element. This represents close drain spacing and relatively long PVDs.

Case D: Vacuum pressure varies linearly along the drain and across the soil element. This represents large drain spacing and lengthy drains.

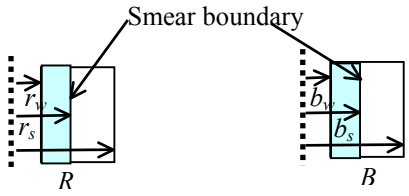

(a) Axisymmetric *(b) Plane strain*

Fig. 1. The unit cell adopted for analytical solution

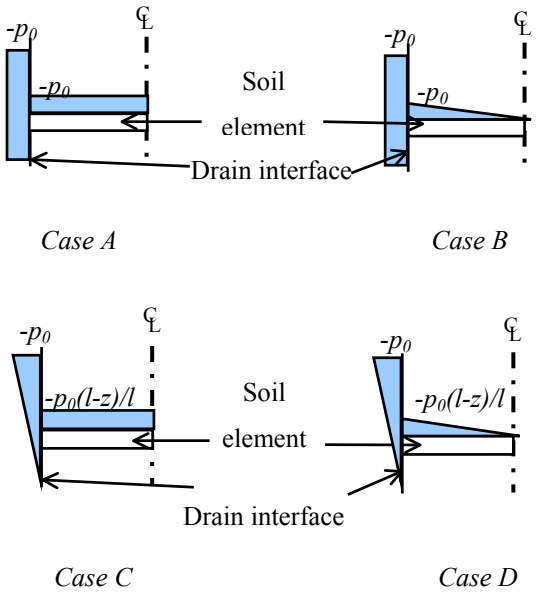

Case A *Case B*

Case C *Case D*

Fig. 2. The distribution patterns of vacuum pressure in the horizontal and vertical directions

Based on the above distributions (Fig. 2), the equations for vacuum pressure at a given point in a unit cell can be given by:

Case A:

$$u_{v,ax}(r,z) = u_{v,ps}(x,z) = p_0 \tag{1a}$$

Case B:

$$u_{v,ax}(r,z) = p_0(R-r)/(R-r_w),$$
$$u_{v,ps}(x,z) = p_0(B-x)/(B-b_w) \tag{1b}$$

Case C:

$$u_{v,ax}(r,z) = u_{v,ps}(x,z) = p_0(l-z)/l \tag{1c}$$

Case D:

$$u_{v,ax}(r,z) = p_0(R-r)(l-z)/l/(R-r_w),$$
$$u_{v,ps}(x,z) = p_0(B-x)(l-z)/l/(B-b_w) \tag{1d}$$

where, $u_{v,ax}(r,z)$ = vacuum pressure at radius r and depth z, p_0 = applied vacuum pressure at the top of the drain, r_w = radius of drain well, l = length of drain, $u_{v,ps}(x,z)$ = vacuum pressure at distance x and depth z, and b_w = width of drain well. Subscripts ax and ps denotes axisymmetric and plane strain condition, respectively.

SOLUTIONS FOR AXISYMMETRIC CONDITION

In this section, for fully saturated soil, the solution for vertical drain incorporating vacuum preloading and smear effects based on Hansbo's solution (1981) is illustrated. The corresponding expressions for the average excess pore pressure, $\bar{u}$, at any time factor, $T_{h,ax}$ are given by:

Case A:

$$\bar{u}/\sigma_1 = \left[1+\left(p_{0,ax}/\sigma_1\right)\right]\exp\left\{-8T_{h,ax}/\mu_{ax}\right\} - \left(p_{0,ax}/\sigma_1\right) \tag{2a}$$

Case B:

$$\bar{u}/\sigma_1 = \left[1+\left(p_{0,ax}/\sigma_1\right)G(n)\right]\exp\left\{-8T_{h,ax}/\mu_{ax}\right\} - \left(p_{0,ax}/\sigma_1\right)G(n) \tag{2b}$$

Case C:

$$\bar{u}/\sigma_1 = \left[1+\left(p_{0,ax}/2\sigma_1\right)\right]\exp\left\{-8T_{h,ax}/\mu_{ax}\right\} - \left(p_{0,ax}/2\sigma_1\right) \tag{2c}$$

Case D:

$$\bar{u}/\sigma_1 = \left[1+\left(p_{0,ax}/\sigma_1\right)G(n)/2\right]\exp\left\{-8T_{h,ax}/\mu_{ax}\right\} - \left(p_{0,ax}/\sigma_1\right)G(n)/2 \tag{2d}$$

where,

$$\mu = \alpha_{ax} + \beta_{ax}\left(k_{h,ax}/k'_{h,ax}\right), s = r_s/r_w,$$
$$n = R/r_w,\ G(n) = (n+2)/3/(n+1),$$
$$\alpha_{ax} = \left\{n^2 \ln(n/s) - \left(n^2-s^2\right)\left(3n^2-s^2\right)/\left(4n^2\right)\right\}/\left(n^2-1\right),$$
$$\beta_{ax} = \frac{1}{\left(n^2-1\right)}\left[\left(n^2 \ln s\right) - \left(s^2-1\right)\left(\frac{4n^2-s^2-1}{4n^2}\right)\right]$$

In the above equations, k_h and k'_h = horizontal permeability

of soil in disturbed and undisturbed zone, respectively, and σ_1 = initial overburden pressure due to preloading.

SOLUTIONS FOR PLANE STRAIN CONDITION

Based on the original study by Indraratna and Redana (1997), the analytical solutions incorporating vacuum preloading and smear effects for plane strain condition are developed here. The solution procedures are similar to the axisymmtric condition. The expression for average excess pore pressure at any time factor, $T_{h,ps}$ for Case A can be expressed by:

$$\bar{u}/\sigma_1 = \left[1+\left(p_{0,ps}/\sigma_1\right)\right]\exp\left\{-8T_{h,ps}/\mu_{ps}\right\} - \left(p_{0,ps}/\sigma_1\right) \quad (3a)$$

For Case B:

$$\bar{u}/\sigma_1 = \left[1+\left(p_{0,ps}/\sigma_1\right)/2\right]\exp\left\{-8T_{h,ps}/\mu_{ps}\right\} - \left(p_{0,ps}/\sigma_1\right)/2 \quad (3b)$$

For Case C:

$$\bar{u}/\sigma_1 = \left[1+\left(p_{0,ps}/\sigma_1\right)/2\right]\exp\left\{-8T_{h,ps}/\mu_{ps}\right\} - \left(p_{0,ps}/\sigma_1\right)/2 \quad (3c)$$

For Case D:

$$\bar{u}/\sigma_1 = \left[1+\left(p_{0,ps}/\sigma_1\right)/4\right]\exp\left\{-8T_{h,ps}/\mu_{ps}\right\} - \left(p_{0,ps}/\sigma_1\right)/4 \quad (3d)$$

where ,

$$\mu = \alpha_{ps} + \left(k_{h,ps}/k'_{h,ps}\right)\beta_{ps},\ \alpha_{ps} = 2\left(n-s\right)^3 \Big/ \left[3n^2\left(n-1\right)\right],$$

$$\beta_{ps} = 2\left\{3n^2\left(s-1\right) - 3n\left(s^2-1\right) + s^3 - 1\right\} \Big/ \left\{3n^2\left(n-1\right)\right\},$$

$$s = b_s/b_w,\ n = B/b_w$$

EFFECT OF MAGNITUDE AND DISTRIBUTION OF VACUUM PRELOADING

In this section, the effects of magnitude and the distribution patterns of vacuum pressure are discussed. Input parameters used in the analysis are n = 9, s=3 and k_h/k'_h=10. The comparison of normalised excess pore water pressure ratio among the 4 vacuum pressure distributions is shown in Fig. 3 (VPR = 1 was used in this analysis). The results predicted by Eqns. (3a) to (3d) are compared with the case of 'no vacuum' application. As expected, the dissipation of excess pore water pressure with applied vacuum pressure in Cases A to D is faster than the case without any vacuum pressure application. It is clear that the application of vacuum pressure increases the lateral pore pressure gradient, promoting radial flow. The excess pore pressure dissipates faster in Case A compared to Case D. It can be seen that the consideration of varied vacuum pressure along the drain length is more realistic, as the effect of vacuum pressure usually diminishes with depth. For long vertical drains, it is possible that the applied vacuum pressure at the drain top may not be felt towards the bottom part of the drain. Figure 4 illustrates the effects of the magnitude of applied vacuum pressure in Case D. The analytical result for the case of VPR = 2.0 shows that the rate of consolidation is more rapid in comparison with VPR = 0.5. Also, it is clear that the greater the magnitude of vacuum pressure, the higher the rate of consolidation. Unless the magnitude of vacuum pressure is large enough (e.g. VPR $\geq$ 1.0), the effect on pore pressure dissipation may not be significant. From the above analyses, it can be noted that the efficiency of the vertical drain incorporating vacuum preloading depends on both the distribution pattern and magnitude of vacuum pressure.

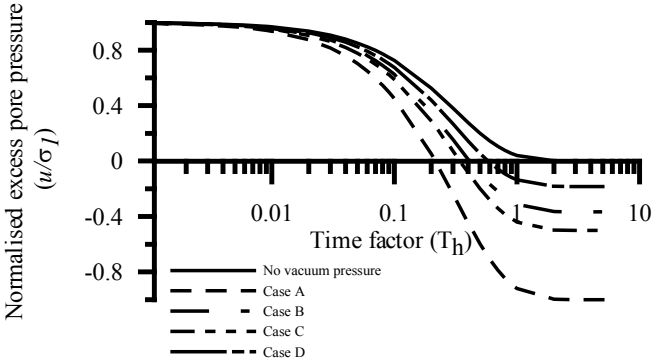

Fig. 3. Comparison of normalised excess pore pressure in different vacuum pressure distribution patterns (Axisymmetric)

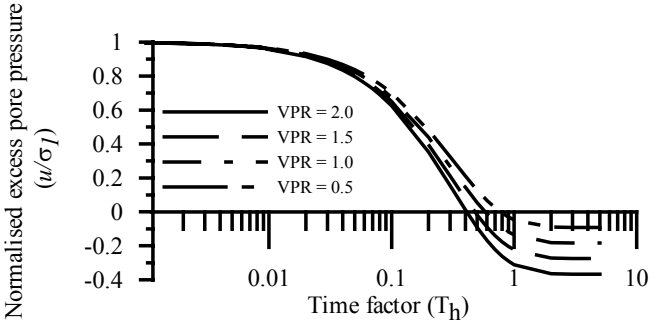

Fig. 4. Effect of different vacuum pressure ratios on the normalised excess pore pressure (Axisymmetric)

COMPARISON BETWEEN AXISYMMETRIC AND PLANE STRAIN ANALYSES

In general, the 'matching' procedure used in vertical drain modeling is useful in the parametric conversion from the true axisymmetric condition (3D) to the assumed plane strain condition employed in 2D finite element analysis. In the past, numerous attempts have been made to determine the most appropriate numerical and analytical procedures to establish the minimum disparity between the axisymmetric and plane strain methods (Hird et al., 1992, Indraratna and Redana, 1997). For vacuum preloading, the proposed 'matching' procedures can be based on the equivalent average excess pore

pressure and the equivalent vacuum pressure by maintaining the same geometry ($r_w = b_w, r_s = b_s \; and \; R = B$). In this study, permeability and vacuum pressure relationships between the axisymmetric and equivalent plane strain conditions have been revised from the original theory developed by Indraratna and Redana (1997). In the equivalent plane strain condition, the magnitudes of $R, r_s \; and \; r_w$ in axisymmetric condition are assumed to be equal to $B, b_s \; and \; b_w$, respectively, which result in the following expression for the equivalent plane strain permeability and vacuum pressure:
Equivalent permeability for undisturbed zone:

$$k_{h,ps} = 0.67 k_{h,ax} / \left[ln(n) - 0.75 \right] \quad (4)$$

Equivalent permeability for smear zone:

$$k'_{h,ps} = \left\{ \beta_{ps} / \left(\alpha_{ax} + \beta_{ax} k_{h,ax} / k'_{h,ax} - \alpha_{ps} \right) \right\} k_{h,ps} \quad (5)$$

Equivalent vacuum pressures:
(i) Cases A and C

$$p_{0,ps} = p_{0,ax} \quad (6a)$$

(ii) Cases B and D

$$p_{0,ps} = 2G(n) p_{0,ax} \quad (6b)$$

APPLICATION OF THE MODEL TO SELECTED EMBANKMENTS

Site Characteristics and Embankment Details

The Second Bangkok International Airport is located in Samutprakan Province, about 30 km east of the capital city, Bangkok. Subsoil layer at this site is composed of a thick soft clay deposit. During the wet season, the area is mostly flooded, which causes high compressibility of the soil, once the pore pressures start to dissipate. Ground improvement with prefabricated vertical drain (PVD) has been studied successfully by using conventional sand surcharge load (Indraratna and Redana, 2000). Since this site is located far from the source of surcharge material, the use of vertical drains incorporating vacuum preloading was introduced as an alternative to reduce the amount of fill material required for embankment construction at this site.

In this study, the soil profile at the site has been divided into 5 sublayers. The subsoil is relatively uniformed, consisting of a top weathered crust (1 m depth) overlying very soft to soft dark gray layers extending from 1 m to 10.5 m depth. A 2.5 m thick medium clay layer underlies the soft clay layer. Underneath the medium clay layer, a light-brown stiff clay layer can be found at 14 m to 21 m depth. The groundwater level varies from 0.5 m to 1 m depth. The initial piezometric level is lower than the theoretical hydrostatic pore pressure at 6.0 m below the ground level, due to the excessive withdrawal of groundwater .

Two test embankments, TV1 and TV2, were constructed on soft Bangkok clay with PVDs. Total base area of each embankment is 40 m × 40 m (Asian Institute of Technology, 1995). For Embankment TV1 (Fig. 4), 15 m long PVDs with hypernet drainage system were used. For Embankment TV2 (Fig. 5), 12 m long PVDs with perforated and corrugated pipes combined with nonwoven geotextile were utilised. The drainage blanket which serves as a working platform was constructed with a thickness of 0.3 m and 0.8 m for TV1 and TV2, respectively. A water and air tight LLDPE geomembrane liner was placed on top of the drainage system. The geomembrane liner was sealed by placing the edges of the bottom of the perimeter trench and covered with 300 mm layer of seal bentonite and submerged under water. The PVDs were installed in a triangular pattern with 1 m spacing. The parmeters of PVD are listed in Table 1.

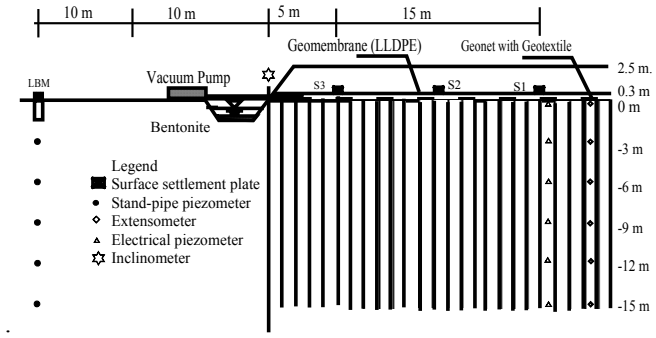

Fig. 5. Cross section of embankment TV1 and location of monitoring system

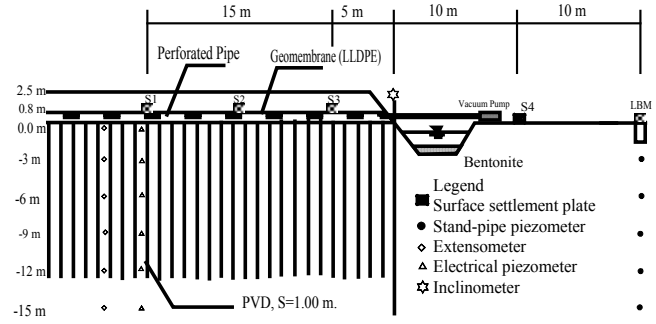

Fig. 5. Cross section of embankment TV2 and location of monitoring system

Table 1. Vertical drain parameters

Spacing, S	1.0 m (triangular)
Diameter of drain, d_w	50 mm
Diameter of smear zone, d_s	300 mm
Ratio of k_h/k'_h	10
Length of vertical drain	15 m for TV1 and 12 m for TV2
Discharge capacity, q_w	50 m^3/year (per drain)

In each embankment, a vacuum pump capable of generating 70 kPa suction pressure was employed. After 45 days of vacuum pressure application, the embankment load was applied in 4 stages upto a height of 2.5 m (the unit weight of surcharge fill equals to 18 kN/m^3). The stages of loading for both embankments are illustrated in Fig.7. Surface settlement plates, subsurface multipoint extensometers, vibrating wire electrical piezometers and inclinometers were installed to monitor the behaviour of the embankments. The surface settlement plates were placed directly on top of the geomembrane. At the edges of each embankment, an inclinometer was installed. The vibrating wire piezometers were installed under the test embankment at 3 m depth intervals together with the sensors for the multipoint piezometer. At the dummy area, observation wells and stand pipe piezometers were also installed. The settlement, excess pore water pressure and lateral movement were monitored for about 150 days.

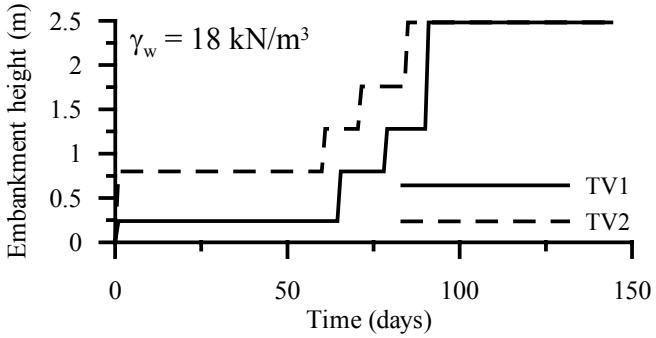

Fig. 7. Multistage loading for embankments TV1 and TV2

Numerical Analysis Incorporating Vacuum Pressure

The numerical analysis was based on the modified Cam-Clay model (Roscoe and Burland, 1968) and the equivalent plane strain Eqns. (4) and (5) developed by the authors, which are incorporated in the finite element code, ABAQUS. The adopted parameters of 5 subsoil layers are listed in Table 2. The critical-state soil properties were determined by Asian Institute of Technology (AIT, 1995). According to the laboratory tests conducted by Indraratna and Redana (1998), the ratio between horizontal and vertical permeability within the smear zone was set to 1. Outside the smear zone, the horizontal permeability was taken to be twice times that of the vertical permeability. For the plane strain simulation, the equivalent permeability inside and outside the smear zone was calculated by Eqns. (4) and (5) for both embankments (Table 3). The discharge capacity (q_w) of 50 m^3/year was derived by using Eqn. (7) which gave an equivalent plane strain permeability, $k_{w,ps}$, of the drain as proposed earlier by Hird et al. (1992).

$$k_{w,ps} = q_w / 2b_w \qquad (7)$$

The equivalent band drain diameter was 50 mm. The diameter of the smear zone was taken to be 300 mm.

Table 2. Modified Cam-Clay parameters

Depth m	λ	κ	ν	e_0	γ kN/m^3
0.0-1.0	0.3	0.03	0.3	1.8	16
1.0-8.5	0.7	0.08	0.3	2.8	15
8.5-10.5	0.5	0.05	0.25	2.4	15
10.5-13	0.3	0.03	0.25	1.8	16
13-15	1.2	0.1	0.25	1.2	18

Table 3. Undisturbed and smear zone equivalent permeability for Embankments TV1 and TV2

Depth m	k_v 10^{-9} m/s	k_h 10^{-9} m/s	k'_h 10^{-9} m/s	$k_{h,ps}$ 10^{-10} m/s	$k'_{h,ps}$ 10^{-10} m/s
0.0-1.0	15.1	30.1	15.1	89.8	6.8
1.0-8.5	6.4	12.7	6.4	38.0	2.9
8.5-10.5	3.0	6.0	3.0	18.0	1.4
10.5-13	1.3	2.6	1.3	7.6	0.6
13-15	0.3	0.6	0.3	1.8	0.1

The finite element mesh, which contains 8-node bi-quadratic displacement and bilinear pore pressure elements, is shown in Fig. 8. Because of symmetry, it was sufficient to consider one half of the embankment for the numerical analysis. For the area with PVDs and smear zone, a finer mesh was employed so that each unit cell represents a single drain and the smear zone on either side of the drain. The finer mesh also prevents unfavorable aspect ratio of elements. The embankment loading was simulated by applying incremental vertical loads to the upper boundary (see Fig. 7).

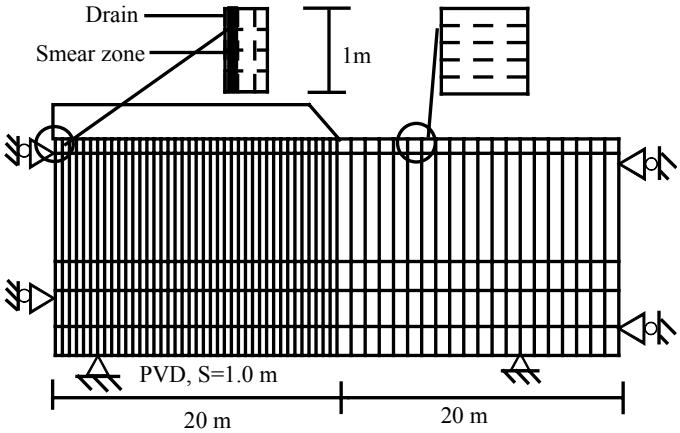

Fig. 8. Finite element mesh for plane strain analysis

Simulation of Vacuum Consolidation

In this section application of Eqn. (6) in conjunction with ABAQUS is demonstrated to simulate vacuum consolidation, and analyse the settlements and lateral displacements. The field measurements are then compared with the numerical

prediction. Figure 9 illustrates the measured pore pressure at various depths of Embankment TV2. After 40 days, there were discrepancies between the measured and applied vacuum pressure. The suction head in the field decreased because of possible air leaks. Therefore, in the analysis, the assumed vacuum pressure value was adjusted based on the field measurements. Figure 10 shows the variation of applied vacuum pressure at the surface, assumed for both embankments. The applied vacuum pressure patterns were divided into 4 cases as explained earlier (Fig. 2), i.e. Cases A to D.

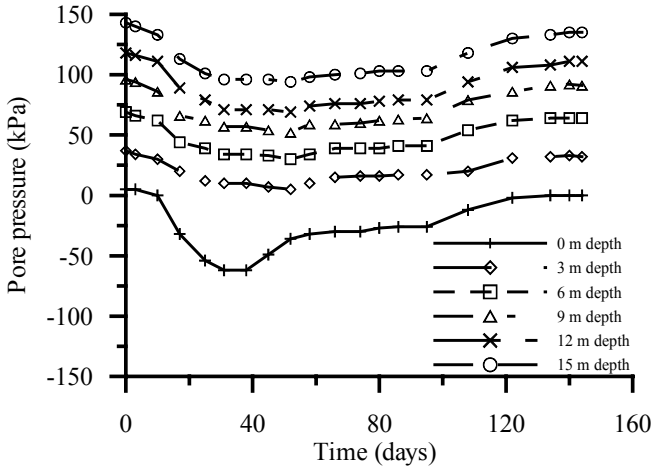

Fig. 9. Pore pressure of embankment TV2 at various depths

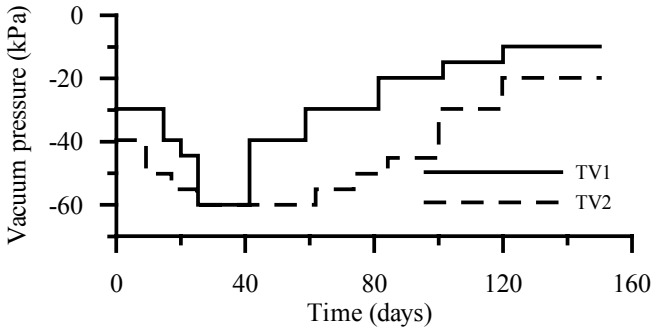

Fig. 10. Vacuum pressure values applied in the analysis

Based on plane strain multidrain analysis, Figure 11 illustrates the comparison between the predicted surface centerline settlement and the measured data (embankment TV1) for Cases A to D as well as for no vacuum application. The predicted results from Case C agree well with the measured results (Fig. 12). For Embankment TV2, the predicted and measured surface settlement results at the centerline of the embankment are shown in Fig. 13. Similar to embankment TV1, Case C models the settlement of this embankment well (Fig.14). Comparing all categories of vacuum pressure distribution, Case A and 'no vacuum pressure' give the highest and lowest settlement, respectively. It is shown that the vacuum application in conjunction with a vertical drain system can accelerate the consolidation process.

From the above analyses, it may be concluded that, for the relatively long PVDs, the effect of vacuum pressure application may diminish along the length of the drain and, if the PVDs are installed closely, the vacuum effect may propagate along the horizontal direction. From the field measurements and FEM analysis, it is clear that the pattern of vacuum distribution directly influences the soil consolidation behaviour, hence the accuracy of the numerical predictions are governed by the correct assumption of vacuum pressure distribution in both vertical and lateral directions.

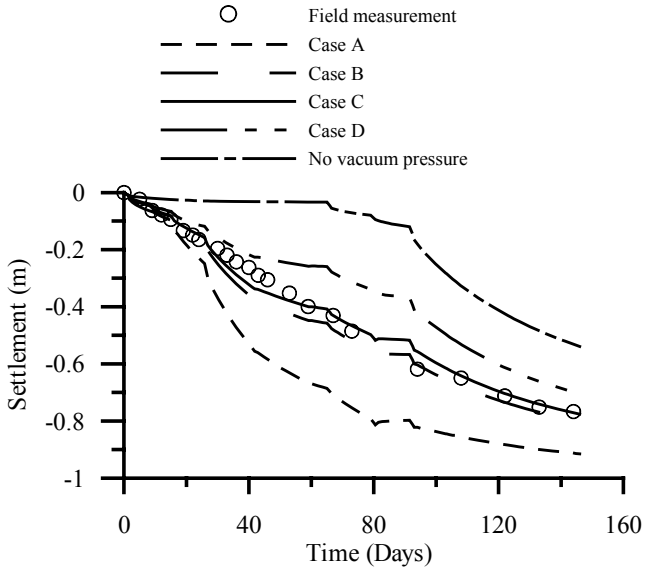

Fig 11. Surface settlement of embankment TV1

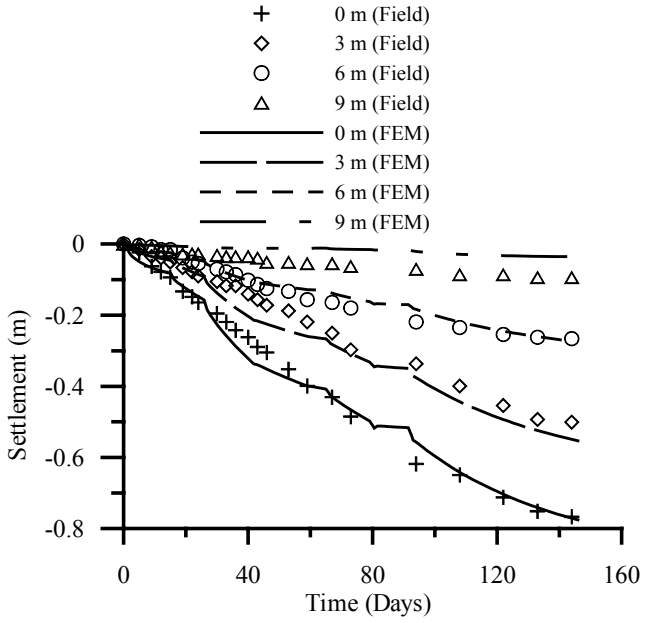

Fig. 12. Consolidation settlement of embankment TV1 (Case C)

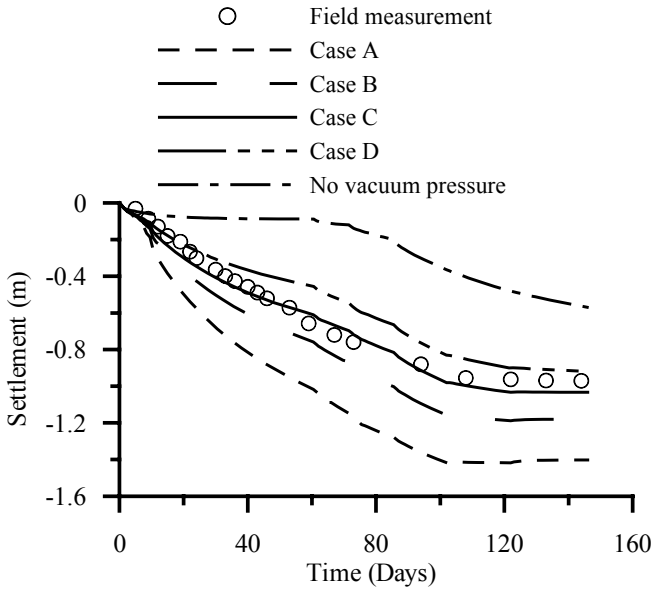

Fig 13. Surface settlement of embankment TV2

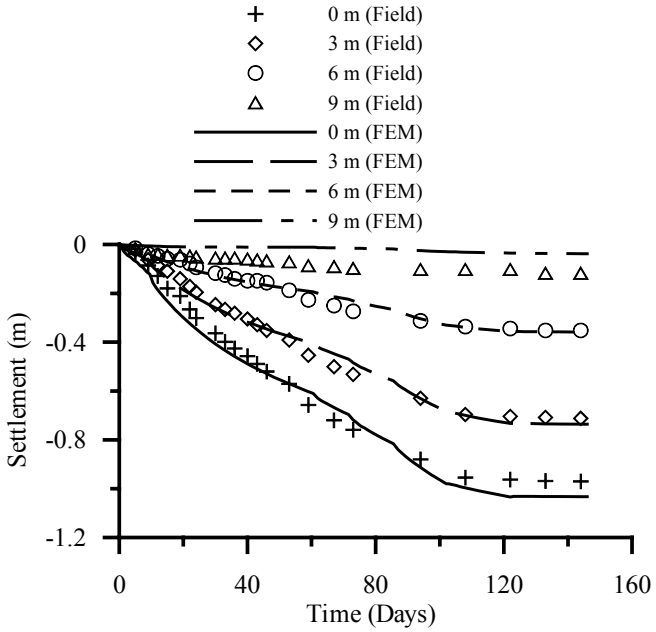

Fig. 14. Consolidation settlement of embankment TV2 (Case C)

The comparisons between predicted and measured lateral movement at the end of construction for Cases A to D plus 'no vacuum pressure' case for embankments TV1 and TV2 are shown in Figs. 15 and 16, respectively. For embankment TV1, the predicted results for Case D at depth below 4 m agrees well with the measurements. However, closer to the ground surface, the field observations do not support the significant 'inward' lateral movements as reflected by the numerical predictions. For embankment TV2, the predicted lateral movement for Case C agrees well with field data at depth below 2 m. However, the discrepancies between the predicted and measured results occur mainly at the weathered crust layer (about 0-2 m depth) for both embankments. This implies that the vacuum pressure effect at the relatively stiff crust needs to be modeled more accurately using highly over-consolidated properties. Previous studies on embankments constucted on soft clay have shown that the accurate prediction of lateral movement is a difficult task, in comparison with vertical displacement (Tavenas et al., 1979). The errors made in the prediction of lateral movements can be numerous. The behaviour of stiff crust cannot be modelled using the conventional modified Cam-Clay properties (Indraratna et al., 1994). In addition, the comparison between the cases of with and without vacuum application confirms that the vacuum preloading definitely causes an inward lateral movement towards the embankment centerline.

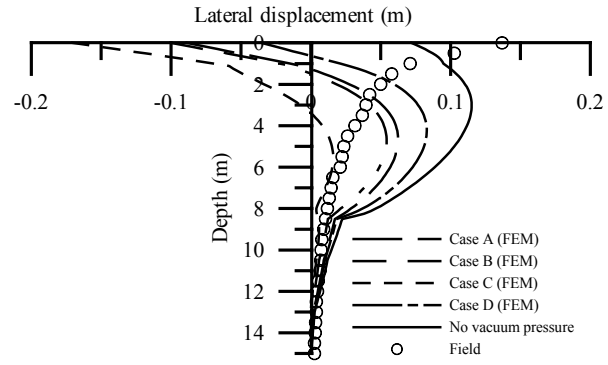

Fig.15. Calculated and measured lateral displacements at embankment TV1

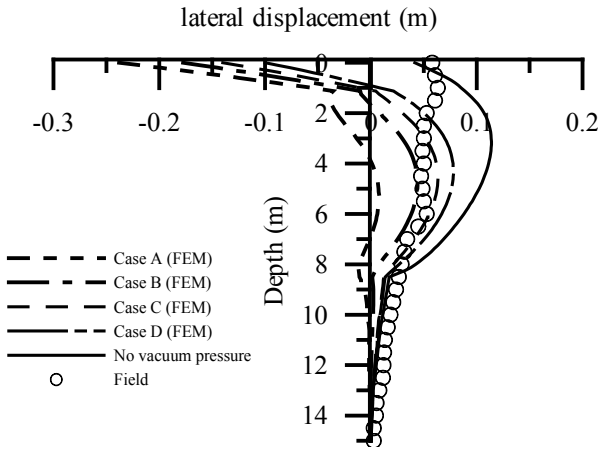

Fig. 16 Calculated and measured lateral displacements at embankment TV2

CONCLUSIONS

Analytical modeling for vertical drains incorporating vacuum preloading and smear effect has been developed for both axisymmetric and plane strain conditions, simulating the consolidation of a unit cell surrounding a single vertical drain. Four distinct distribution patterns for vacuum preloading were considered in the numerical model. The results indicated that the efficiency of vertical drains depends on the magnitude of

vacuum pressure and its distribution in the vertical and lateral directions. Subsequently, a matching procedure based on the transformation of permeability and applied vacuum pressure was introduced to establish the relationships between the axisymmetric and the equivalent plane stain conditions.

A multidrain plane strain model was executed to evaluate the performance of soft clay beneath 2 embankments. The effect of both smear and well resistance associated with the prefabricated vertical drains were considered in the analysis, in conjunction with vacuum pressure. By employing the proposed matching procedure, the centerline settlement at different depths and lateral movement were analyzed and compared to the available field data. For both embankments, the predictions of Case C vacuum distribution agreed well with the field measurement. This implies that the vacuum pressure will decay along the drain length, while probably remaining constant across the soil in the lateral direction if the drain spacing is close enough. Therefore, Case C model is most suitable for a dense pattern of PVDs that are relatively long (i.e. drain length > 15 m, and spacing of the drain around 1 m).

The accurate prediction of lateral displacement requires careful assessment of soil properties, especially for the topmost weathered crust. The vacuum application substantially decreases the lateral displacement, thereby minimizing the risk of shear failure. It can be concluded that the system of vertical drains (PVD) incorporating vacuum preloading is a useful method for accelerating the consolidation settlement and for reducing the amount of surcharge load required otherwise to obtain the same consolidation rate. However, the effectiveness of vacuum system depends on the air leak protection in the field. While the finite element simulation is regarded as a practical tool to predict the performance of soft clay stabilized by PVDs, the accurate modeling of the effect of vacuum preloading requires further research and insight to the vacuum pressure distribution mechanisms via PVD. The length and spacing of PVD play a significant influence in this regard

ACKNOWLEDGEMENTS

The authors greatfully appreciate the cooperation of the Airports Authority of Thailand (AAT). They wish to extend their thanks also to Asian Institute of Technology for providing relevant field data reports.

REFERENCES

Asian Institute of Technology [1995]. "*The full-scale field test of prefabricated vertical drains for the Second Bangkok International Airport: Final report*", Vol. 1, Asian Institute of Technology, Thailand.

Baron, R.A. [1948]. "Consolidation of fine-grained soils by drain wells", *Trans. ASCE*, Vol. 113, pp.718-754.

Chu, J., Yan, S.W., and Yang, H. [2000]. "Soil improvement by the vacuum preloading method for an oil storage station', *Geotechnique*, Vol. 50, No.6, pp. 625-632.

Hansbo, S. [1981]. "Consolidation of fine-grained soils by prefabricated drains and lime column installation", *Proc. 10th International Conference on SMFE*, Vol. 3, pp. 677-682.

Hird, C.C., Pyrah, I.C. and Russel, D. [1992]. "Finite element modeling of vertical drains beneath embankments on soft ground", *Geotechnique*, Vol. 42, No. 3, pp. 499-511.

Indraratna, B., Balasubramanium, A.S. and Ratnayake, P. [1994]. "Performance of embankment stabilized with vertical drains on soft clay*", Journal of Geotechnical Engineering*, ASCE, Vol. 120, No. 2, pp. 257-273.

Indraratna, B. and Redana, I.W. [1997]. "Plane strain modeling of smear effects associated with vertical drains*", Journal of Geotechnical and Geoenvironmental Engineering*, Vol. 123, No. 5, pp. 474-478.

Indraratna, B. and Redana, I.W. [1998]. "Laboratory determination of smear zone due to vertical drain installation*", Journal of Geotechnical Engineering*, ASCE, Vol. 123, No.5, pp. 474-478.

Indraratna, B. and Redana, I.W. [2000]. 'Numerical modeling of vertical drains with smear and well resistance installed in soft clay", *Canadian Geotechnical Journal*, Vol. 37, pp. 133-145.

Kjellman, W. [1952]. "Consolidation of clayey soils by means of atmospheric pressure", *Proceedings of a conference on Soil Stabilization*, Massachusetts Institute of Technology, Cambridge, Ma, pp. 258-263.

Mohamedelhassan, E. and Shang, J.Q. [2002]. "Vacuum and surcharge combined one-dimensional consolidation of clay soils", *Canadian Geotechnical Journal*, Vol. 39, pp. 1126-1138.

Roscoe, K.H. and Burland, J.B. [1968]. "On the generalized stress-strain behaviour of wet clay", *Engineering Plasticity*, pp. 535-569.

Shang, J.Q., Tang, M., Miao, Z. [1998]. "Vacuum preloading consolidation of reclaimed land: a case study", *Canadian Geotechnical Journal*, Vol. 35, pp. 740-749.

Tavenas, F., Mieussens, C. and Bourges, F. [1979]. "Lateral displacements in clay foundations under embankments", *Canadian Geotechnical Journal*, Vol. 16, pp. 532-550.